Oxygenated products formed from OH-initiated reactions of trimethylbenzene: Autoxidation and accretion

Yuwei Wang[1], Archit Mehra[2], Jordan E. Krechmer[3], Gan Yang[1], Xiaoyu Hu[1], Yiqun Lu[1], Andrew Lambe[3],

Manjula Canagaratna[3], Jianmin Chen[1], Douglas Worsnop[3], Hugh Coe[2], Lin Wang[1,4,5] *

[1] Shanghai Key Laboratory of Atmospheric Particle Pollution and Prevention (LAP[3]), Department of Environmental Science and Engineering, Jiangwan Campus, Fudan University, Shanghai 200438, China
[2] Centre for Atmospheric Science, School of Earth and Environment Sciences, The University of Manchester, Manchester, M13 9PL, UK
[3] Center for Aerosol and Cloud Chemistry, Aerodyne Research Inc., Billerica, MA, USA
[4] Collaborative Innovation Center of Climate Change, Nanjing 210023, China
[5] Shanghai Institute of Pollution Control and Ecological Security, Shanghai 200092, China

Corresponding Author: L.W., email, lin_wang@fudan.edu.cn; phone, +86-21-31243568

Abstract. Gas-phase oxidation pathways and products of anthropogenic volatile organic compounds (VOCs), mainly aromatics, are the subject of intensive research with attention paid to their contributions to secondary organic aerosol (SOA) formation and potentially, new particle formation (NPF) in the urban atmosphere. In this study, a series of OH-initiated oxidation experiments of trimethylbenzene (TMB, C_9H_{12}) including 1,2,4-TMB, 1,3,5-TMB, 1,2,3-TMB, and 1,2,4-(methyl-D3)-TMBs ($C_9H_9D_3$) were investigated in an oxidation flow reactor (OFR), in the absence and presence of NO_x. Products were measured using a suite of state-of-the-art instruments, i.e., a nitrate-based chemical ionization - atmospheric pressure interface time-of-flight mass spectrometer (Nitrate CI-APi-TOF), an iodide-adduct chemical ionization - time-of-flight mass spectrometer (Iodide CI-TOF) equipped with a Filter Inlet for Gases and AEROsols (FIGAERO), and a Vocus proton-transfer-reaction mass spectrometer (Vocus PTR). A large number of C9 products with 1-11 oxygen atoms and C18 products presumably formed from dimerization of C9 peroxy radicals were observed, hinting the extensive existence of autoxidation and accretion reaction pathways in the OH-initiated oxidation reactions of TMBs. Oxidation products of 1,2,4-(methyl-D3)-TMBs with deuterium atoms in different methyl substituents were then used as a molecular basis to propose potential autoxidation reaction pathways. Accretion of C9 peroxy radicals is the most significant for aromatics with meta-substituents and the least for aromatics with ortho-substituents, if the number and size of substituted groups are identical. The presence of NO_x would suppress the formation of C18 highly oxygenated molecules (HOMs) and enhance the formation of organonitrates, and even dinitrate organic compounds. Our results show that the oxidation products of TMB are much more diverse and could be more oxygenated than the current mechanisms predict.

1 Introduction

Oxidation products of volatile organic compounds (VOCs) contribute significantly to the formation of secondary organic aerosols (SOAs) (Ng et al., 2010; Zhang et al., 2007), which raises a globally ubiquitous health and environmental concern (Hallquist et al., 2009). There have been numerous studies that aim to construct detailed VOC oxidation mechanisms to advance our understanding on VOC degradation, SOA formation, and ozone formation (Atkinson, 1986; Atkinson and Arey, 2003; Atkinson and Carter, 1984; Kroll and Seinfeld, 2008; Ziemann and Atkinson, 2012). Based on the hypothesis that the products and

43   kinetics of many unstudied chemical reactions can be proposed by analogy to known reactions of similar

44   chemical species (Ziemann and Atkinson, 2012) and/or predicted by the structure-activity relationships

45   (Kwok and Atkinson, 1995), the Master Chemical Mechanism (MCM) is developed as a nearly explicit

46   chemical mechanism, describing the degradation of numerous VOCs (Bloss et al., 2005; Jenkin et al., 2003;

47   Saunders et al., 2003). Due to the high complexity of VOC oxidation processes, it is not surprising that

48   mechanisms leading to the formation of previously unidentified species are still missing.

49   The formation of highly oxygenated organic molecules (HOMs) through the autoxidation pathway

50   during VOC oxidation is such an example. HOMs refer to organic compounds typically containing six or

51   more oxygen atoms that are formed in the gas phase (Bianchi et al., 2019). Autoxidation is a chemical

52   process where an alkyl peroxy radical (RO_2) undergoes an intramolecular hydrogen shift followed by

53   addition of a molecular oxygen, resulting in a more oxygenated RO_2 radical (Crounse et al., 2013; Ehn et

54   al., 2014). It is an effectively repetitive uni-molecular reaction as the more oxidized RO_2 will serve as a

55   parent RO_2 in the next autoxidation reaction, leading to the rapid formation of HOMs in very short time

56   scales (Bianchi et al., 2019; Jørgensen et al., 2016).

57   Owing to recent developments in the analytical techniques such as nitrate-anion chemical ionization

58   mass spectrometry (nitrate CIMS), our knowledge on the autoxidation pathway during the oxidation of

59   biogenic volatile organic compounds (BVOCs) has been significantly improved. Certain systems, such as

60   the oxidation of monoterpenes, have been studied extensively, of which ozonolysis has been confirmed as

61   an important source for HOMs (Ehn et al., 2014; Jokinen et al., 2014). The OH-initiated oxidation is also a

62   considerable HOM formation source for monoterpenes and isoprene (Krechmer et al., 2015), albeit at lower

63   yields for monoterpenes containing an endocyclic double bond (Jokinen et al., 2014, 2015; Rissanen et al.,

64   2015). Detailed mechanisms of monoterpene-derived HOM formation reactions, initiated by ozone or OH,

65   were investigated through theoretical calculations (Berndt et al., 2016), or by analogy to reactions of similar

66   chemical species, i.e., cyclohexene (Rissanen et al., 2014). A couple of studies performed H/D isotope

67   exchange experiments, which can probe the number of hydrogen atoms other than that in C-H, strongly

68   supporting the proposal of autoxidation mechanisms (Ehn et al., 2014; Rissanen et al., 2014). Research on

69   other BVOCs, i.e., isoprene and sesquiterpenes (Crounse et al., 2013; Richters et al., 2016; Teng et al.,

70   2017), and on other oxidants, i.e., NO_3 and chlorine (Nah et al., 2016; Wang et al., 2019), indicate the

71   widespread existence of autoxidation pathways in the oxidation of BVOCs. The products formed from

72   autoxidation of biogenic precursors have been proven to play a vital role in atmospheric new particle

73   formation (NPF) because of their low volatility (Ehn et al., 2014; Stolzenburg et al., 2018; Tröstl et al.,

74   2016).

75   On the other hand, studies on autoxidation of anthropogenic VOCs are rather sparse. Wang et al. (2017)

76   theoretically and experimentally showed the autoxidation route of alkylbenzenes to form HOMs in the gas

77   phase. Identities and yields of HOM products from different aromatics were systematically measured and

78   the determined molar HOM yields were in the range of 0.1 % to 2.5 %, which are similar to the molar HOM

79   yields of OH-initiated reactions of BVOCs (Jokinen et al., 2015; Molteni et al., 2018). Currently, aromatics-

80   derived HOMs are believed to be formed via many reaction pathways, including accretion, bicyclic

81   intermediate reactions, and multi-generation OH reactions (Berndt et al., 2018b; Garmash et al., 2019;

82   Zaytsev et al., 2019). The unimolecular isomerization and autoxidation reactions of aromatic peroxy

83   radicals have been shown to be fast enough to compete with other bimolecular reactions even under NO

84   concentrations as high as in urban environment (Tsiligiannis et al., 2019).

85   Trimethylbenzene (TMB) including isomers of 1,3,5-TMB, 1,2,3-TMB, and 1,2,4-TMB is one of the

86   most common anthropogenic VOCs in urban areas. OH-initiated oxidation of TMB is its dominant chemical

87   loss in the atmosphere (Atkinson and Arey, 2003), which proceeds either via H atom abstraction from the

88   methyl substituents or via addition of OH radical onto the aromatic ring (Ziemann and Atkinson, 2012).

89   The H atom abstraction channel is minor in the OH-induced oxidation reactions of TMB, forming dimethyl-

90   benzaldehyde. The major channels of OH addition consist of peroxide-bicyclic pathway, phenolic pathway,

91   and epoxy-oxy pathway (Bloss et al., 2005; Calvert et al., 2002; Jenkin et al., 2003). The three TMB isomers

92   have different branching ratios for these pathways resulting from the substitution-, site-, and stereo-

93   specificity, however specific branching ratios are still in debate. Among these pathways, the peroxide-

94   bicyclic pathway has the highest branching ratio and can form bicyclic peroxy radicals (BPRs), which are

95   important intermediates that contribute significantly to the formation of HOMs (Wang et al., 2017).

96   Subsequent reactions of the intermediates will lead to the formation of stabilized products. On the other

97   hand, the details of the autoxidation mechanisms for anthropogenic precursors remain elusive. Direct

98   measurements of individual H-shift rates, the detailed structure of HOMs, and a robust quantification of

99   HOM yields are still lacking. The detailed kinetics for termination reactions of different RO_2 are also

100   ambiguous. Consequently, it is hard to comprehensively judge the TMB oxidation reaction pathways and

101   products under different atmospheric conditions, and to evaluate the contribution of TMB oxidation to

102   atmospheric NPF and SOA formation.

103   In this study, we studied the OH-initiated oxidation of 1,3,5-TMB, 1,2,3-TMB, and 1,2,4-TMB with

104   a focus on autoxidation and accretion products, via the concurrent usage of a Vocus proton-transfer-reaction

105   time-of-flight mass spectrometry (Vocus PTR), an iodide-adduct chemical ionization - time-of-flight mass

106   spectrometer equipped with a Filter Inlet for Gases and AEROsols (FIGAERO Iodide CI-TOF), and a

107   nitrate-based chemical ionization - atmospheric pressure interface time-of-flight mass spectrometer (Nitrate

108   CI-APi-TOF). Oxidation of 1,2,4-(methyl-D3)-TMBs was investigated to elucidate the detailed

109   autoxidation reaction pathway. The influence of NO_x concentration on product distribution was also
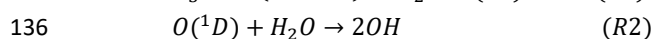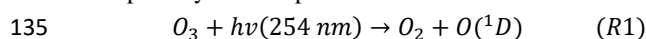
110   investigated.
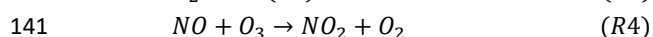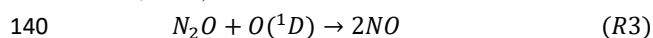
111

112   2 Methods

113   As shown in Figure 1, oxidation experiments of TMB were conducted in a Potential Aerosol Mass

114   (PAM) oxidation flow reactor (OFR, Aerodyne Research, Inc.). A self-prepared VOC cylinder was used to

115   provide a constant source of gaseous TMB as a reactant. O_3/OH was produced in-situ in the PAM and the

116   relative humidity (RH) was regulated by the PAM setup, which will be introduced in details later. A Vocus

117   PTR (Krechmer et al., 2018), a FIGAERO Iodide CI-TOF (Lee et al., 2014; Lopez-Hilfiker et al., 2014),

118   and a Nitrate CI-APi-TOF (Ehn et al., 2014; Eisele and Tanner, 1993) were deployed to detect gaseous

119   products as well as particulate ones. In addition, an ozone monitor (Model 106-M, 2B technologies) and a

120   NO_x monitor (Model 42i-TLE; Thermo Fisher Scientific) were utilized to measure trace gas concentrations,

121   whereas a set of Scanning Mobility Particle Sizer (SMPS, consisting of one TSI Model 3080 Long DMA

122   and one TSI Model 3776 Condensation Particle Counter) was employed to measure the number size

123   distribution of submicron aerosol particles.

124   **OFR.** In this study, the sum of all the flows in the PAM, including a zero air flow, an ozone (O_3) flow,
125   a TMB/N_2 flow, and a N_2O/N_2 flow depending upon experimental conditions, was kept at either 10 or 10.4
126   slpm (standard litres per minute, standard to 0 ℃, 1 atm), resulting in calculated mean residence times of
127   approximately 80 seconds. Zero air was generated by a zero gas generator (Sabio Model 1001 Zero Gas
128   Source). A fraction of the zero air was passed through a Nafion humidifier (Perma Pure Model FC100-80-
129   6MSS) filled with ultrapure water to achieve the desired RH in the OFR. Ozone was generated by passing
130   800 sccm (standard cubic centimetre, standard to 0 ℃, 1 atm) of zero air through a separate ozone chamber
131   and input into the OFR. In order to create a low HO_2/RO_2 ratio environment to promote the carbonyl and
132   hydroxyl channels to terminate RO_2 radicals, the OFR was operated with only the 254 nm lights on (Lambe
133   et al., 2019), which is referred to as OFR254 mode in previous studies (Peng et al., 2015). In OFR254 mode,
134   the primary oxidant production reactions in the OFR are:
135           $O_3 + hv(254\ nm) \rightarrow O_2 + O(^1D)$ (R1)
136           $O(^1D) + H_2O \rightarrow 2OH$ (R2)
137   In some experiments, N_2O (99.999%, Air Liquide) was added at the OFR inlet, corresponding to
138   mixing ratios of 3.4% of the total gas flow rates, which produced NO_x via the following reactions (Lambe
139   et al., 2017):
140           $N_2O + O(^1D) \rightarrow 2NO$ (R3)
141           $NO + O_3 \rightarrow NO_2 + O_2$ (R4)
142   Before each experiment, the PAM OFR was purged with zero air under the OFR254 operation mode
143   until the signals of acetic acid and other common VOC oxidation products decreased to background levels
144   of the Vocus PTR and CI-TOF that are described below.
145   **Vocus PTR.** The newly developed Vocus PTR has a high sensitivity to a wide range of VOCs and
146   oxygenated volatile organic compounds (OVOCs) (Krechmer et al., 2018; Li et al., 2019; Riva et al., 2019).
147   Its mass resolving power (m/Δm = ~12000 at 200 Th, 1 Th = 1 u/e, where e is the elementary charge and
148   u is the atomic mass unit) allows to simultaneously monitor many isobaric species, and even to distinguish
149   the very minor mass discrepancy (0.001548 u) between one deuterium atom and two hydrogen atoms. The
150   instrument background together with a quantitative calibration by injection of standards was measured
151   between every two experiments to minimize potential inaccuracies. In our study, the pressure of the
152   focusing ion-molecule reactor (FIMR) was actively maintained at 1.5 mbar resulting in an E/N of the FIMR
153   at 110 Td (1 Td = 1×10^{-17} V cm^2), which was generally a moderate operating condition leading to relatively
154   little fragmentation of compounds of interest (Gueneron et al., 2015; Yuan et al., 2017).
155   **FIGAERO-Iodide CI-TOF.** The Iodide-adduct CI-TOF is able to determine elemental compositions
156   of a suite of atmospheric oxygenated organic species (D'Ambro et al., 2017; Lee et al., 2014; Lopez-Hilfiker
157   et al., 2016). It has increasing sensitivities toward more polar and acidic VOCs (Lee et al., 2014). The mass
158   resolution of the Iodide CI-TOF was tuned to be around 3000. The reagent ion (I^-) was produced from
159   permeated CH_3I vapor in N_2 by a radioactive source of Am-241 (0.1 mCi). The pressure in the ion-molecule
160   reactor (IMR) was regulated at 100 mbar, whereas the small segmented quadrupole (SSQ) pressure was set
161   to be around 2 mbar. The FIGAERO inlet manifold enables the Iodide CI-TOF to measure both gas and
162   particle compositions at a molecular level (Lopez-Hilfiker et al., 2014). In our study, aerosols were collected
163   onto a PTFE filter (5µm, Millipore) at 0.96 slpm for 20 min, while the gases were measured simultaneously

164   via a separate dedicated port. Then, a thermal desorption cycle was started 2 minutes after the FIGAERO

165   filter was aligned to a heating tube, through which a heated ultra-high purity nitrogen flow was passed and

166   heated according to a pre-programmed temperature ramp. The ultra-high purity nitrogen was initially held

167   at 25 °C for 2 min, and then heated at a rate of 10 °C min^{-1} to 200 °C, which was maintained for the

168   remainder of the temperature ramp (50 min in total).

169   **Nitrate CI-APi-TOF.** The Nitrate CI-APi-TOF has been increasingly used for the measurement of

170   low volatility organic compounds (LVOC) and extremely low volatility organic compounds (ELVOCs)

171   (Ehn et al., 2014; Hyttinen et al., 2015; Jokinen et al., 2014), which mostly have a high O:C ratio. The

172   resolving power of the Nitrate CI-APi-TOF was up to around 8000 in our study. The selectivity of nitrate

173   ions keeps the spectrum clean from the more abundant, less oxidized compounds in our experiments. Most

174   of the detected species were observed exclusively as adducts with NO_3^-, a very minor fraction of which

175   contain odd hydrogen numbers and are hence postulated to be radicals but not presented in this manuscript.

176   The concurrent use of three mass spectrometers (MSs) with different reagent ions allows us to obtain

177   a comprehensive picture of the oxidation products of TMB with OH radicals. The detection suitability of

178   these three instruments for oxidation products with various levels of oxidation has been discussed a lot in

179   previous studies (Isaacman-VanWertz et al., 2017; Krechmer et al., 2018; Riva et al., 2019). Generally,

180   Vocus PTR displays selectivity for less oxidized compounds; Iodide CI-TOF favors more oxygenated

181   species; and Nitrate CI-APi-TOF shows the highest efficiency for the most oxidized compounds. Dimer

182   products of TMB oxidation are expected to be detected by Nitrate CI-APi-TOF as clusters with NO_3^-, which

183   is due to the potential hydrogen bond donor functional groups in these molecules, inferred from the

184   abundant oxygen and hydrogen atoms in the formulas. These products should not be detected by Vocus

185   PTR. One explanation is that these molecules are likely to be fragile and therefore have fragmented owing

186   to the protonation or the strong electric field in the FIMR of Vocus PTR. Alternatively, these products

187   might not go through the PEEK tube inlet of Vocus PTR. At the same time, the sample inlet for Iodide CI-

188   TOF in our experiments is not desirable for the detection of dimer products.

189   To ensure that the reported signal is truly from the sample flow instead of internal background or

190   contamination, subtraction of the mass spectra for the OFR background from the samples has been

191   performed for each instrument. In addition, since this study is mostly concerned with identification of

192   oxidation products from OH-initiated reactions of TMBs and elucidation of the potential autoxidation

193   pathway, Nitrate CI-APi-TOF and Iodide CI-TOF were hence not calibrated and only the arbitrary signals

194   with MS transmission correction (Heinritzi et al., 2016; Krechmer et al., 2018) were compared within the

195   same instrument. It should then be noted that the relative signal intensities are biased among the MSs

196   because of their ionization methods and transmission efficiency.

197   In each experiment, the Vocus PTR was used to confirm the establishment of stable precursor gas

198   concentrations, and then the pair of 254 nm Hg lamps were turned on to generate the OH radicals and

199   reaction products were analyzed by the MSs. The input RH in the OFR was kept at a low level and the

200   voltage of the Hg lamps was slightly tuned in every experiment, so that the OH exposure in the OFR was

201   close to one oxidation lifetime of TMB (Kurylo and Orkin, 2003), i.e., consumption of 62.3% of the initial

202   TMB. Under this condition, the production of the first-generation products is generally favored, if the

203   subsequent loss reactions for these products are assumed to proceed in the same rate.

204   Table 1 summarizes all the experiments that were performed. Studied were 1,3,5-TMB ($\geq$ 99.0%,
205   Aladdin), 1,2,3-TMB (Analytical standard, Aladdin), 1,2,4-TMB ($\geq$ 99.5%, Aladdin), 1,2,4-(1-methyl-
206   D3)-TMB ($\geq$ 95%, Qingdao Tenglong Weibo Technology Co., Ltd., China), 1,2,4-(2-methyl-D3)-TMB ($\geq$
207   95%, Qingdao Tenglong Weibo Technology Co., Ltd., China), and 1,2,4-(4-methyl-D3)-TMB ($\geq$ 95%,
208   Qingdao Tenglong Weibo Technology Co., Ltd., China). The structure of these partially deuterated TMBs
209   can be found in Figure S1. Note that ozone reactions were not taken into account in this study, because
210   ozone reacts with aromatics at negligible rates, and its reaction rate with oxidation products containing C=C
211   double bonds is much slower compared with that of OH (Jenkin et al., 1997, 2003; Molteni et al., 2018;
212   Saunders et al., 2003).

3 Results and discussion

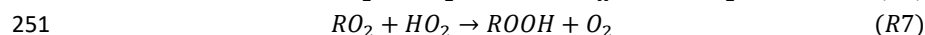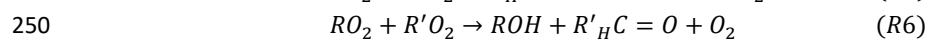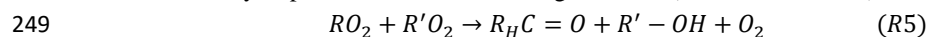### 3.1 Characteristics of C9 products

216   Figure 2 presents an overview of C7, C8 and C9 products in a carbon oxidation state ($\overline{OS}_C$)-carbon
217   number (n_C) space as observed by three MSs and also those predicted by MCM v3.3.1. Carbon oxidation
218   state is a quantity that increases with the level of oxidation, which reveals the chemical aging of atmospheric
219   organics (Kroll et al., 2011). It is evident that more species were detected by the three MSs, and although
220   there were clear differences between products detected from different MSs, results indicate missing
221   oxidation pathways in the current versions of the MCM (MCM v3.3.1, available at:
222   http://mcm.leeds.ac.uk/MCM). Oxygen-containing C9 products were formed by adding functional groups
223   to the carbon skeleton, whereas C7 and C8 products resulted from carbon-carbon scission of the original
224   carbon skeleton together with functionalization. A large proportion of C7-C9 products were more oxidized
225   than those predicted by MCM, hinting the existence of highly efficient oxidation pathways. At the same
226   time, some of the C7 and C8 products were characterized with unexpected low $\overline{OS}_C$, of which a few were
227   even less oxidised than the precursor. The observation of these products is another indication for the
228   existence of missing pathways in the current oxidation mechanisms.

229   Recent studies have emphasized on the importance of the peroxide-bicyclic pathway in producing
230   highly oxygenated compounds in the oxidation of alkylbenzenes (Wang et al., 2017; Zaytsev et al., 2019),
231   which leads to the formation of ring-retaining products. Therefore, here we further investigated C9 products
232   of TMB oxidation detected by the three MSs (Figure 3). $C_9H_{10}O_{1-6}$, $C_9H_{12}O_{1-7}$, and $C_9H_{14}O_{4-6}$ contributed
233   to the most of the signal intensities in Vocus PTR (Figure 3a). Compounds with fewer hydrogen atoms than
234   TMB in Vocus PTR might be formed from hydrogen abstraction reactions. Iodide CI-TOF detected
235   products with five to seven oxygen atoms (Figures 3b & 3c), which is narrower compared with Vocus PTR
236   and Nitrate CI-APi-TOF. Molecules with 18 hydrogen atoms were detected only in Iodide CI-TOF, which
237   is an unexpected high number. These molecules, low in signal intensities in both gas and particle phases,
238   might be formed from multiple OH attacks since each OH attack can only add two hydrogens in maximum
239   onto the parent molecule. The species with the highest signal intensities measured in the gas phase appeared
240   to be $C_9H_{12}O_4$, $C_9H_{12}O_6$, $C_9H_{14}O_5$, and $C_9H_{14}O_6$ in the 1,2,4-TMB + OH experiment, $C_9H_{14}O_5$ and $C_9H_{14}O_6$
241   in the 1,3,5-TMB + OH experiment, and $C_9H_{12}O_6$ and $C_9H_{12}O_7$ in the 1,2,3-TMB + OH experiment (Figure
242   3b). Compared with the gas phase, more oxidized particulate products tended to contribute a larger
243   proportion of signal in FIGAERO-Iodide-CI-APi-TOF (Figure 3c). Nevertheless, the gas phase products

Atmospheric
Chemistry
and Physics
Discussions

244   are emphasized in the current study, which can be detected by and compared among the three instruments.

245   Nitrate CI-APi-TOF detected C9 products containing 12-16 hydrogen atoms and 5-11 oxygen atoms (Figure

246   3d).

247   RO_2 radicals can react in the absence of NO, to form termination products including carbonyls,

248   alcohols, and hydroperoxides via the following reactions (Mentel et al., 2015).

249            $RO_2 + R'O_2 \rightarrow R_H C = O + R' - OH + O_2$ (R5)

250            $RO_2 + R'O_2 \rightarrow ROH + R'_H C = O + O_2$ (R6)

251            $RO_2 + HO_2 \rightarrow ROOH + O_2$ (R7)

252   Here we present a criteria method based on the work of Mentel et al. (2015). For a parent peroxy radical

253   with a molecular mass of m, its termination ought to lead to the formation of a carbonyl, an alcohol, and a

254   hydroperoxyl, which have a molecular mass of m-17, m-15, and m+1, respectively. Since elemental

255   formulas as determined by the high-resolution MS do not contain information regarding functional groups

256   or the structure of a molecule, the identified mass spectral signals could be counted as either one of the

257   three categories. Listed in Table 2 are detected stabilized oxidation products in categories of carbonyl,

258   alcohol, and hydroperoxyl, which hints the potential existence of the corresponding peroxy radicals. These

259   stabilized products all contain six or more oxygen atoms, which meet the definition of HOMs (Bianchi et

260   al., 2019). $C_9H_{12}O_6$ is the only signal that has been predicted by MCM, assumed to be a hydroperoxyl

261   product from a ring-opening peroxy radical that goes through multiple OH attack reactions (MCM name:

262   C7MOCOCO3H), which is unlikely to occur under our experimental conditions. Four pairs of peroxy

263   radicals, i.e., $C_9H_{13}O_7\bullet$ and $C_9H_{13}O_9\bullet$, $C_9H_{13}O_8\bullet$ and $C_9H_{13}O_{10}\bullet$, $C_9H_{15}O_7\bullet$ and $C_9H_{15}O_9\bullet$, and $C_9H_{15}O_8\bullet$ and

264    $C_9H_{15}O_{10}\bullet$, can be selected from the eight potential peroxy radicals in Table 2. The molecular formulas for

265   the peroxy radicals within each pair differ by $2 \times O$, which is a first evidence for the autoxidation pathway.

266

267   **3.2 Autoxidation mechanisms of 1,2,4-TMB**

268   The autoxidation pathways were then further elucidated by experiments with isotopically labelled

269   precursors, 1,2,4-(1-methyl-D3)-TMB, 1,2,4-(2-methyl-D3)-TMB, and 1,2,4-(4-methyl-D3)-TMB, whose

270   structure is shown in Figure S1.

271   If an intramolecular hydrogen shift happens during autoxidation with the abstracted hydrogen coming

272   from a methyl group, molecular oxygen will rapidly attach to this carbon-centred radical to form a new

273   alkyl peroxy radical (Bianchi et al., 2019 and reference herein). One potential fate of this R-CH$_2$OO• radical

274   is to lose one of the two remaining hydrogen atoms, forming a carbonyl according to Reaction R5. Thus,

275   one of the three original hydrogen atoms in the methyl group will leave this molecule after an autoxidation

276   step (Ehn et al., 2014; Mentel et al., 2015; Molteni et al., 2018; Otkjær et al., 2018; Rissanen et al., 2014;

277   Wang et al., 2017). In the case of a deuterium abstraction from a methyl-D3 group during the autoxidation,

278   an oxidation product with two deuterium atoms ($C_xH_yD_2O_z$) will then be formed, which is presumably a

279   carbonyl. Although an alcohol or a hydroperoxyl could also be formed from a peroxy radical, it is not

280   suitable to utilize the presence of alcohol and hydroperoxyl products as a criteria to judge the existence of

281   autoxidation. The hydroxyl channel of deuterated peroxy radicals can lead to the formation of alcohol

282   products with either 3 or 4 deuterium atoms, depending on the nature of the other reacting RO_2. The slow

283   unimolecular reaction rate of deuterated methyl group corresponds to little formation of the products with

Atmospheric
Chemistry
and Physics
Discussions

Open Access

EGU

284   4 deuterium atoms, whereas our MSs cannot differentiate 3 deuterium atoms either from a molecule with

285   autoxidation and hydroxyl termination or from an untouched methyl-D3 group. On the other hand, the

286   hydroperoxyl channel would lead to the formation of hydroperoxyl products with 3 deuterium atoms, too.

287   Therefore, only the carbonyl channel products of a peroxy radical was used to suggest the potential

288   autoxidation that has occurred.

289   Table 3 summaries two-deuterium-containing C9 ($C_9H_yD_2O_z$) products that were detected by Vocus

290   PTR and Nitrate CI-APi-TOF in different isotope labelling experiments: $C_9H_{10}D_2O_6$ in the 1,2,4-(1-methyl-

291   D3)-TMB + OH experiment by Vocus PTR and Nitrate CI-APi-TOF; $C_9H_{10}D_2O_7$ in the 1,2,4-(1-methyl-

292   D3)-TMB + OH experiment by Vocus PTR; and $C_9H_{12}D_2O_8$ in the 1,2,4-(4-methyl-D3)-TMB + OH

293   experiment by Nitrate CI-APi-TOF. $C_9H_{10}O_7D_2$ (234.0703 Th) was expected to be detected by Nitrate CI-

294   APi-TOF, but unfortunately an undefined peak (located at 295.9827 Th) covered the position where

295   $C_9H_{10}O_7D_2 \cdot NO_3^-$ (296.0592 Th) was supposed to been identified. $C_9H_{12}D_2O_8$ (252.0814 Th) was not

296   detected by Vocus PTR, likely owing to either its low proton affinity or its partitioning onto the inlet of

297   Vocus PTR , given its high O:C ratio and hence low volatility. However, Nitrate CI-APi-TOF was able to

298   detect this very sticky compound, because the nitrate source is constructed with concentric sample and

299   sheath flows that minimize the diffusive losses of samples to the source wall. These results indicate that an

300   intramolecular deuterium-migration happened on the 1-methyl-D3 substituent of the $C_9H_{10}D_3O_4$ and

301   $C_9H_{10}D_3O_5$ radicals, and the 4-methyl-D3 substituent of the $C_9H_{12}D_3O_7$ radical, respectively, then one

302   oxygen was added to the resulting alkyl radicals, and the new peroxy radical reacted to form $C_9H_{10}D_2O_6$,

303   $C_9H_{10}D_2O_7$, and $C_9H_{12}D_2O_9$, respectively.

304   These three compounds ($C_9H_{10}D_2O_6$, $C_9H_{10}D_2O_7$, and $C_9H_{12}D_2O_9$) did not possess high signal

305   intensities, because the deuterium transfer reactions are typically significantly slower for D (^2H) nuclei than

306   hydrogen transfer reactions for H (^1H) (Bianchi et al., 2019; Wang et al., 2017). There might be other two-

307   deuterium-containing C9 products in these experiments. However, since many of these signals were at the

308   instrument detection limits or even lower, the nonideal experimental conditions prevent us from confirming

309   more such compounds.

310   Based on the observed signals of two-deuterium-containing C9 products and structures that have been

311   previously proven to favor H-shift reactions (Otkjær et al., 2018), two plausible formation pathways for the

312   observed products are proposed.

313   The first one starts with a BPR of $C_9H_{13}O_5\cdot$ as shown in Scheme 1, which is the first BPR formed from

314   C_9H_{12} via the peroxide-bicyclic pathway. The structure of this particular $C_9H_{13}O_5\cdot$ is different from what is

315   proposed in MCM v3.3.1, but the position for the initial OH attack, i.e., the 4th carbon on the ring, is feasible

316   owing to the attraction of a substituted group on its para-position (Li and Wang, 2014), and the subsequent

317   addition of O_2 after the initial OH attack along with bicyclization occurs on the same relative position as

318   previous studies have suggested (Bloss et al., 2005; Jenkin et al., 2003). The resulting BPR of

319   $C_9H_{13}O_5\cdot$ undergoes a hydrogen shift, during which the abstracted hydrogen comes from the methyl

320   terminal of an allylic group. This hydrogen is much easier to be abstracted, compared to those in a normal

321   methyl group that are unlikely to go through a hydrogen shift with a peroxy radical (Otkjær et al., 2018).

322   The new BPR of $C_9H_{13}O_7\cdot$ then reacts via R5, R6, and R7 to form $C_9H_{12}O_6$, $C_9H_{14}O_6$, and $C_9H_{14}O_7$,

323   respectively. This pathway is suggested by the observation of $C_9H_{10}D_2O_6$ in the 1,2,4-(1-methyl-D3)-TMB

324   + OH experiment. On the other hand, $C_9H_{13}O_5\cdot$ can alternatively self-react or react with a HO_2 radical to

Atmospheric
Chemistry
and Physics
Discussions

Open Access

EGU

325   form an alkoxy intermediate, which goes through isomerization and addition of an oxygen to form a BPR
326   of $C_9H_{13}O_8\bullet$. The stabilized products from $C_9H_{13}O_8\bullet$ include $C_9H_{12}O_7$, $C_9H_{14}O_7$, and $C_9H_{14}O_8$. This pathway
327   is suggested by the observation of $C_9H_{10}D_2O_7$ in the 1,2,4-(1-methyl-D3)-TMB + OH experiment.

328   It's noted that in all the three isotope experiments, we also detected products of $C_9H_9D_3O_6$ and
329    $C_9H_9D_3O_7$ with much higher signal intensities, indicating the existence of other autoxidation pathways.
330   Thus, it deserves a repeated emphasis here that we only point out feasible pathways that are supported by
331   our isotope experiments in this work, but do not rule out other possibilities.

332   The second pathway is described in scheme 2. This pathway starts from a BPR of $C_9H_{13}O_5\bullet$ that is
333   formed by the initial OH attack and subsequent reactions. MCM v3.3.1 includes a BPR with the same
334   structure but does not contain the subsequent reactions. The BPR of $C_9H_{13}O_5\bullet$ can be terminated via R5,
335   forming a stabilized hydroxyl product of $C_9H_{14}O_4$, which is subject to a second OH attack and a following
336   addition of O_2, resulting in a new peroxy radical of $C_9H_{15}O_7\bullet$. There are no systematic investigations on the
337   effect of a peroxide-bicyclic substitution on the 1,5 H-shift rate constant. However, our data indicate a
338   hydrogen shift can occur on the 4-methyl group, based on which the structure of $C_9H_{15}O_9\bullet$ is proposed. The
339   new BPR of $C_9H_{15}O_9\bullet$ is then terminated via R5, R6, and R7, forming stabilized products $C_9H_{14}O_8$, $C_9H_{16}O_8$,
340   and $C_9H_{16}O_9$, respectively. This pathway is suggested by the observation of $C_9H_{12}D_2O_8$ in the 1,2,4-(4-
341   methyl-D3)-TMB + OH experiment, though other pathways could result in products with the same formula.

3.3 Characteristics of C18 HOMs

344   Products with 18 carbon atoms were observed in our experiments by Nitrate CI-APi-TOF, all
345   containing 24-30 hydrogen atoms and 8 or more atoms ($C_{18}H_{24/26/28/30}O_{>8}$) (Figure 4). C18 products with 26
346   or 28 hydrogen atoms contributed the most of the signal intensities while those generated by 1,3,5-TMB
347   were the most abundant. Recent studies revealed that long-neglected organic peroxide dimer (ROOR')
348   formation reactions might be an important source of gas-phase dimer compounds, through which two
349   peroxy radicals form accretion products consisting of the carbon backbone of both reactants (Berndt et al.,
350   2018a, 2018b; Zhao et al., 2018).

351    $$RO_2 + R'O_2 \rightarrow ROOR' + O_2 \qquad (R8)$$

352   This reaction has been proved to be another important loss process for RO_2 radicals formed via autoxidation.
353   On account of their extraordinarily low vapor pressure, HOM dimers contribute more significantly to the
354   formation and growth of atmospheric new particles than HOM monomers.

355   Our C18 oxidation products have similar ion formulas to the dimer products in recent 1,3,5-TMB
356   oxidation experiments (Molteni et al, 2018; Tsiligiannis et al., 2019). In our experiments, the formation of
357    $C_{18}H_{26}O_{8-15}$, $C_{18}H_{28}O_{9-15}$, and $C_{18}H_{30}O_{12-15}$ can be explained by reactions of two $C_9H_{13}O_x\bullet$, one $C_9H_{13}O_x\bullet$ and
358   one $C_9H_{15}O_x\bullet$, and two $C_9H_{15}O_x\bullet$ respectively. $C_{18}H_{24}O_{8-13}$ with low signal intensities were detected by
359   Nitrate CI-APi-TOF, hinting that H-abstraction reactions have occurred leading to a lower hydrogen atom
360   in the product than in the precursor.

361   Figure 5 summarizes the relative contribution of C9 and C18 products formed from TMB oxidation as
362   detected by Nitrate CI-APi-TOF. The charge efficiency for C9 and C18 products is assumed to be identical
363   in Nitrate CI-APi-TOF. Hence, the measured relative abundances of the oxidation products, with
364   corrections of the transmission function in the MS, can faithfully represent the product distribution in the

365 experiments. In the Exp. #1-3, the dimers ($C_{18}H_{26}O_{8-15}$) formed from two $C_9H_{13}O_x$· along those ($C_{18}H_{28}O_{9-15}$) from one $C_9H_{13}O_x$· and one $C_9H_{15}O_x$· contributed the most intensity, whereas the most intensive C9 products ($C_9H_{14}O_{5-11}$) could be the alcohol or hydroperoxyl products of $C_9H_{13}O_x$·, or the carbonyl products of $C_9H_{15}O_x$· (Table S1). 1,2,3-TMB produced the most C9 products, 1,2,4-TMB the second, and 1,3,5-TMB the least. An opposite trend was observed for C18 products. Therefore, the reduction of C9 products was likely due to the dimer formation. Here, we define the C18 fraction as the ratio of the signal intensities of C18 products to the sum of those of C9 and C18 products in Nitrate CI-APi-TOF, and the C9 fraction in a similar way. According to our results, the dimer fraction was the highest for aromatics with meta-substituents and the least for aromatics with ortho-substituents, if the number and size of substituted groups are identical, while the monomer fraction had an opposite tendency. This can be explained by the stereoselectivity of accretion formation reactions.

376 Under our experimental conditions, the C18 dimer fraction in the 1,3,5-TMB experiments was around 86.5%, which is much higher than the dimer fraction of 42.6%-56.5% re-calculated using the measured C9 and C18 signals by Tsiligiannis et al. (2019), 43.3%-52.4% modelled by Tsiligiannis et al. (2019), and 39% reported by Molteni et al. (2018t). The lack of a m/z-transmission correction in the former two studies could partially explain the discrepancy (Molteni et al., 2018; Tsiligiannis et al., 2019). On the other hand, this observation could also be due to the much higher RO_2 concentrations in our experiments. The amount of reacted 1,3,5-TMB in our experiment is around 74.1 ppb (~ 1.8×10^{12} molecules cm^{-3}), whereas in the experiments of Tsiligiannis et al. (2019) and Molteni et al. (2018), the numbers are 26 ppb (~ 6.5×10^{11} molecules cm^{-3}) and 22.3 ppb (~5.6×10^{11} molecules cm^{-3}), respectively.

3.4 Influence of NO_x

387 Figure 6 describes the distribution of C9 products detected by Nitrate CI-APi-TOF in the absence of NO_x (Exp. #1), a low NO_x experiment (Exp. #7), and a higher NO_x experiment (Exp. #8), respectively. Once NO_x was added, the formation of C9 non-nitrogen products declined down to around 20% of those in Exp. #1. The production of C9 non-nitrogen products did not decrease much between low NO_x experiment and higher NO_x experiment, indicating a nonlinear effect of NO_x on the production of C9 non-nitrogen products. Dinitrates ($C_9H_xN_2O_y$) increased with the NO_x concentration, but C9 organonitrates (ONs, $C_9H_xNO_y$) slightly reduced in the higher NO_x experiment compared to that in the low one, which indicates a complex competition between $RO_2 + RO_2$ and $RO_2 + NO_x$.

395 The observation of C9 products containing 1-2 nitrogen atoms and C18 products with one nitrogen atom is similar to the results for 1,3,5-TMB oxidation experiments in the presence of NO_x reported by Tsiligiannis et al. (2019). NO_x can perturb the fate of peroxy radicals by the following reactions (Orlando and Tyndall, 2012; Rissanen, 2018):

399 $$RO_2 + NO \rightarrow RONO_2 \qquad (R9)$$
400 $$RO_2 + NO_2 \rightarrow RO + NO_2 \qquad (R10)$$
401 $$RO_2 + NO_2 \rightarrow RO_2NO_2 \qquad (R11)$$
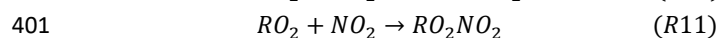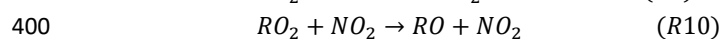
402 Competing with the other RO_2 reactions, NO_x can dramatically reduce the formation of C9 non-nitrogen products. The NO_x levels in the low NO_x experiment (Exp. #7) and higher NO_x experiment (Exp. #8) were

404 0.8 ppb and 6.5 ppb, respectively. Compared to the ambient values in polluted areas, this NO_x/VOC is low.

405 The NO_x/(ΔVOC) was around 0.8% in the low NOx experiment and 6.4% in higher NO_x one.

406 Most organonitrates observed in our study were characterized with 13 hydrogen atoms, as detected by

407 Nitrate CI-APi-TOF (Figure S2). All of them contained more than 6 oxygen atoms, with molecular formulas

408 corresponding to bicyclic organonitrates formed from termination reactions of $C_9H_{13}O_x$• with NO or NO_2

409 (i.e., pathway R9 and R11, respectively). The dinitrates were dominated by species with 14 hydrogen atoms

410 (Figure S3). As suggested by Tsiligiannis et al. (2019), an OH radical could attack a nitrated compound

411 that is formed from NO_x termination of a peroxy radical, then an oxygen atom is added (similarly to the

412 reactions from $C_9H_{14}O_7$ to $C_9H_{15}O_7$ in scheme 2), and then the newly formed peroxy radical that have

413 already contained one nitrogen will be terminated by NO or NO_2 again. Therefore, most of the detected

414 dinitrates were also formed from $C_9H_{13}O_x$•.

415 Figure 7a describes the relative intensities of C18 HOMs in Exp. #7, and Exp. #8 as detected by Nitrate

416 CI-APi-TOF, in comparison with their relative intensities in Exp. #1. The relative intensities of most of the

417 C18 HOMs decreased with the NO_x/(ΔVOC), while a few of the C18 HOMs including $C_{18}H_{24}O_{13}$, $C_{18}H_{26}O_{13}$,

418 $C_{18}H_{26}O_{14}$, $C_{18}H_{28}O_{12}$ increased slightly in the higher NO_x experiment, potentially from a combined effect

419 of NO_x and OH. The injection of NO_x can compete with the other RO_2 reactions, and thus it consumes

420 peroxy radicals that would otherwise go through accretion reactions, which explains the decrease of most

421 C18 HOMs. On the other hand, the introduction of NO_x can increase the oxidation capacity in the OFR, as

422 it does in the ambient environment, leading to the slight enhancement for the few C18 HOMs. After the

423 addition of NO_x, all of the C18 HOMs decreased by more than six times compared with those in no NO_x

424 experiments, indicating that the dimers were more strongly influenced than monomers, which is in

425 agreement with a previous study (Tsiligiannis et al., 2019).

426 The C18 ONs with 25 or 27 hydrogen atoms were detected in the NO_x experiments (Figure 7b). Other

427 C18 products containing nitrogen atoms were not detected. The $C_{18}H_{25}NO_x$ might be formed from reactions

428 between a $C_9H_{12}NO_x$• radical and a $C_9H_{13}O_x$• radical, or between a $C_9H_{14}NO_x$• and a $C_9H_{11}O_x$• radical, all

429 of which existed in the system. The $C_{18}H_{27}NO_x$ is most likely to be formed from reactions between a

430 $C_9H_{14}NO_x$• radical and a $C_9H_{13}O_x$• radical, which were the most abundant C9 radicals. All the C18 ONs

431 decreased with the increase of NO_x/(ΔVOC), which is reasonable. Introduction of NO_x into the system

432 triggered reactions between C9 peroxy radicals and NO_x, which consequently reduced the formation of

433 accretion products like C18 ONs.

434

435 **4 Conclusions**

436 The identities and distribution of oxidation products formed from OH-initiated reactions of three

437 TMBs were obtained with a suite of state-of-the-art chemical ionization mass spectrometers. Our recent

438 study shows that the ring-retaining products are more oxygenated and quite a lot of carbon-carbon scission

439 products are missed in the current model, indicating that the degradation products of aromatics are much

440 more diverse than what is available in MCM (Mehra et al., 2020). Because of its important contribution to

441 the nucleation and SOA formation in urban areas, the ring-retaining products of TMB deserve a more

442 detailed characterization. Here we have built on that work by showing the formation pathways of ring-

443 retaining highly oxygenated products and through identification of accretion products.

444   With the assistance of three 1,2,4-(methyl-D3)-TMB experiments we have demonstrated that the rapid
445 formation of HOMs is attributable to the autoxidation pathway during the TMB oxidation. Several plausible
446 autoxidation pathways for OH-initiated reactions of 1,2,4-TMB were proposed, emphasizing on the ring-
447 retaining pathways of aromatics, especially the bicyclic-peroxide channel, which is followed by
448 autoxidation that is not shown in the current models, such as MCM. Oxidation of aromatic VOCs was
449 shown in our study to produce HOM dimers, which might be underestimated or even completely ignored
450 in previous studies which utilize techniques not capable of detecting dimers. The structural enhancement
451 for accretion product formation via the $RO_2 + R'O_2$ reaction has been observed, of which the meta-
452 substituents was shown to be strongest and ortho-substituents the weakest, though the detailed
453 stereoselectivity for aromatics remains unclear now.

454   In the presence of NO_x whose reaction with $RO_2\cdot$ can compete with $RO_2\cdot + RO_2\cdot$ or $RO_2\cdot +$
455 $HO_2\cdot$ reactions, ONs and dinitrates will be generated via reactions of NO_x with BPRs in 1,2,4-TMB
456 oxidation system, and dimer products with one nitrogen will be formed via the subsequent reactions. This
457 is consistent with a recent ambient observations in the polluted environment, where ONs, dinitrates, and
458 nitrogen-containing dimers presumably formed from BVOCs and alkylbenzenes were detected (Brean et
459 al., 2019). The formation of ONs and dinitrates from TMB is not linearly depending on the NO_x
460 concentration, which excludes the possibility of extrapolating our laboratory results to ambient conditions.
461 Nevertheless, the changes of HOM compositions in the presence of NO_x, especially the accretion products,
462 could have an effect on NPF and SOA formation. Previous work has showed that the ring-retaining product
463 formation at NO_x environment tends to be more important for TMB than other single substituted C9
464 aromatics, i.e., isopropylbenzene and propylbenzene, which emphasized the significance of TMB ring-
465 retaining oxidation in the urban environment (Mehra et al., 2020). Further research is needed to acquire a
466 quantitative understanding of the role of NO_x in HOM formation.

467   Clearly, these multifunctional gas phase products appear at different stages of the oxidation chain.
468 These mass spectra can be used as ideal "fingerprints" of TMB oxidation in the ambient gas phase
469 measurement to elucidate atmospheric oxidation conditions.

470

471 *Data availability.* Data related to this article will be available from a persistent repository and upon request
472 from corresponding authors.

473

474 *Supplement.* The supplement related to this article is available online.

475

476 *Author contributions.* LW, and YW designed the experiments. YW, GY, XH, and YL carried out the
477 instrument deployment and operation. AM, JK, and AL provided technical support. YW analyzed the data.
478 YW, LW, and JK wrote the paper. All co-authors discussed the results and commented on the manuscript.

479

480 *Competing interests.* The authors declare that they have no conflict of interest.

481

References

Atkinson, R.: Kinetics and Mechanisms of the Gas-Phase Reactions of the Hydroxyl Radical with Organic Compounds under Atmospheric Conditions, Chem. Rev., 86(1), 69–201, doi:10.1021/cr00071a004, 1986.

Atkinson, R. and Arey, J.: Atmospheric Degradation of Volatile Organic Compounds, Chem. Rev., 103(12), 4605–4638, doi:10.1021/cr0206420, 2003.

Atkinson, R. and Carter, W. P. L.: Kinetics and Mechanisms of the Gas-Phase Reactions of Ozone with Organic Compounds under Atmospheric Conditions, Chem. Rev., 84(5), 437–470, doi:10.1021/cr00063a002, 1984.

Berndt, T., Richters, S., Jokinen, T., Hyttinen, N., Kurtén, T., Otkjær, R. V., Kjaergaard, H. G., Stratmann, F., Herrmann, H., Sipilä, M., Kulmala, M. and Ehn, M.: Hydroxyl radical-induced formation of highly oxidized organic compounds, Nat. Commun., 7(May), doi:10.1038/ncomms13677, 2016.

Berndt, T., Mentler, B., Scholz, W., Fischer, L., Herrmann, H., Kulmala, M. and Hansel, A.: Accretion Product Formation from Ozonolysis and OH Radical Reaction of α-Pinene: Mechanistic Insight and the Influence of Isoprene and Ethylene, Environ. Sci. Technol., 52(19), 11069–11077, doi:10.1021/acs.est.8b02210, 2018a.

Berndt, T., Scholz, W., Mentler, B., Fischer, L., Herrmann, H., Kulmala, M. and Hansel, A.: Accretion Product Formation from Self- and Cross-Reactions of RO2 Radicals in the Atmosphere, Angew. Chemie Int. Ed., 57(14), 3820–3824, doi:10.1002/anie.201710989, 2018b.

Bianchi, F., Kurtén, T., Riva, M., Mohr, C., Rissanen, M. P., Roldin, P., Berndt, T., Crounse, J. D., Wennberg, P. O., Mentel, T. F., Wildt, J., Junninen, H., Jokinen, T., Kulmala, M., Worsnop, D. R., Thornton, J. A., Donahue, N., Kjaergaard, H. G. and Ehn, M.: Highly Oxygenated Organic Molecules (HOM) from Gas-Phase Autoxidation Involving Peroxy Radicals: A Key Contributor to Atmospheric Aerosol, Chem. Rev., 119(6), 3472–3509, doi:10.1021/acs.chemrev.8b00395, 2019.

Bloss, C., Wagner, V., Jenkin, M. E., Volkamer, R., Bloss, W. J., Lee, J. D., Heard, D. E., Wirtz, K., Martin-Reviejo, M., Rea, G., Wenger, J. C. and Pilling, M. J.: Development of a detailed chemical mechanism (MCMv3.1) for the atmospheric oxidation of aromatic hydrocarbons, Atmos. Chem. Phys., 5(3), 641–664, doi:10.5194/acp-5-641-2005, 2005.

Brean, J., Harrison, R. M., Shi, Z., Beddows, D. C. S., Acton, W. J. F., Nicholas Hewitt, C., Squires, F. A. and Lee, J.: Observations of highly oxidized molecules and particle nucleation in the atmosphere of Beijing, Atmos. Chem. Phys., doi:10.5194/acp-19-14933-2019, 2019.

Calvert, J. G., Atkinson, R., Becker, K. H., Kamens, R., Seinfeld, J., Wallington, T. and Yarwood, G.: The Mechanisms of Atmospheric Oxidation of Aromatic Hydrocarbons., Oxford University Press, Inc., New York, 2002.

Crounse, J. D., Nielsen, L. B., Jørgensen, S., Kjaergaard, H. G. and Wennberg, P. O.: Autoxidation of organic compounds in the atmosphere, J. Phys. Chem. Lett., 4(20), 3513–3520, doi:10.1021/jz4019207, 2013.

D'Ambro, E. L., Lee, B. H., Liu, J., Shilling, J. E., Gaston, C. J., Lopez-Hilfiker, F. D., Schobesberger, S., Zaveri, R. A., Mohr, C., Lutz, A., Zhang, Z., Gold, A., Surratt, J. D., Rivera-Rios, J. C., Keutsch, F. N. and Thornton, J. A.: Molecular composition and volatility of isoprene photochemical oxidation secondary organic aerosol under low- and high-NOx conditions, Atmos. Chem. Phys., 17(1), 159–174, doi:10.5194/acp-17-159-2017, 2017.

Ehn, M., Thornton, J. A., Kleist, E., Sipilä, M., Junninen, H., Pullinen, I., Springer, M., Rubach, F., Tillmann, R., Lee, B., Lopez-Hilfiker, F., Andres, S., Acir, I. H., Rissanen, M., Jokinen, T., Schobesberger, S., Kangasluoma, J., Kontkanen, J., Nieminen, T., Kurtén, T., Nielsen, L. B., Jørgensen, S., Kjaergaard, H. G., Canagaratna, M., Maso, M. D., Berndt, T., Petäjä, T., Wahner, A., Kerminen, V. M., Kulmala, M., Worsnop, D. R., Wildt, J. and Mentel, T. F.: A large source of low-volatility secondary organic aerosol, Nature, 506(7489), 476–479, doi:10.1038/nature13032, 2014.

Eisele, F. L. and Tanner, D. J.: Measurement of the gas phase concentration of H2SO4 and methane sulfonic acid and estimates of H2SO4 production and loss in the atmosphere, J. Geophys. Res., doi:10.1029/93JD00031, 1993.

Garmash, O., Rissanen, M. P., Pullinen, I., Schmitt, S., Kausiala, O., Tillmann, R., Percival, C., Bannan, T. J., Priestley, M., Hallquist, Å. M., Kleist, E., Kiendler-Scharr, A., Hallquist, M., Berndt, T., McFiggans, G., Wildt, J., Mentel, T., Ehn, M. and Garmash olgagarmash, O.: Multi-generation OH oxidation as a source for highly oxygenated organic molecules from aromatics, Atmos. Chem. Phys. Discuss, doi:10.5194/acp-2019-582, 2019.

Gueneron, M., Erickson, M. H., Vanderschelden, G. S. and Jobson, B. T.: PTR-MS fragmentation patterns of gasoline hydrocarbons, Int. J. Mass Spectrom., 379, 97–109, doi:10.1016/j.ijms.2015.01.001, 2015.

Hallquist, M., Wenger, J. C., Baltensperger, U., Rudich, Y., Simpson, D., Claeys, M., Dommen, J., Donahue, N. M., George, C., Goldstein, A. H., Hamilton, J. F., Herrmann, H., Hoffmann, T., Iinuma, Y., Jang, M., Jenkin, M. E., Jimenez, J. L., Kiendler-Scharr, A., Maenhaut, W., McFiggans, G., Mentel, T. F., Monod, A., Prévôt, A. S.

541   H., Seinfeld, J. H., Surratt, J. D., Szmigielski, R. and Wildt, J.: The formation, properties and impact of
542   secondary organic aerosol: Current and emerging issues, Atmos. Chem. Phys., 9(14), 5155–5236,
543   doi:10.5194/acp-9-5155-2009, 2009.
544   Heinritzi, M., Simon, M., Steiner, G., Wagner, A. C., Kürten, A., Hansel, A. and Curtius, J.: Characterization of the
545   mass-dependent transmission efficiency of a CIMS, Atmos. Meas. Tech., 9(4), 1449–1460, doi:10.5194/amt-9-
546   1449-2016, 2016.
547   Hyttinen, N., Kupiainen-Määttä, O., Rissanen, M. P., Muuronen, M., Ehn, M. and Kurtén, T.: Modeling the
548   Charging of Highly Oxidized Cyclohexene Ozonolysis Products Using Nitrate-Based Chemical Ionization, J.
549   Phys. Chem. A, 119(24), 6339–6345, doi:10.1021/acs.jpca.5b01818, 2015.
550   Isaacman-VanWertz, G., Massoli, P., O'Brien, R. E., Nowak, J. B., Canagaratna, M. R., Jayne, J. T., Worsnop, D.
551   R., Su, L., Knopf, D. A., Misztal, P. K., Arata, C., Goldstein, A. H. and Kroll, J. H.: Using advanced mass
552   spectrometry techniques to fully characterize atmospheric organic carbon: current capabilities and remaining
553   gaps, Faraday Discuss., 200, 579–598, doi:10.1039/C7FD00021A, 2017.
554   Jenkin, M. E., Saunders, S. M. and Pilling, M. J.: The tropospheric degradation of volatile organic compounds: A
555   protocol for mechanism development, Atmos. Environ., 31(1), 81–104, doi:10.1016/S1352-2310(96)00105-7,
556   1997.
557   Jenkin, M. E., Saunders, S. M., Wagner, V. and Pilling, M. J.: Protocol for the development of the Master Chemical
558   Mechanism, MCM v3 (Part B): tropospheric degradation of aromatic volatile organic compounds, Atmos.
559   Chem. Phys., 3(1), 181–193, doi:10.5194/acp-3-181-2003, 2003.
560   Jokinen, T., Sipilä, M., Richters, S., Kerminen, V. M., Paasonen, P., Stratmann, F., Worsnop, D., Kulmala, M., Ehn,
561   M., Herrmann, H. and Berndt, T.: Rapid autoxidation forms highly oxidized RO2 radicals in the atmosphere,
562   Angew. Chemie - Int. Ed., 53(52), 14596–14600, doi:10.1002/anie.201408566, 2014.
563   Jokinen, T., Berndt, T., Makkonen, R., Kerminen, V. M., Junninen, H., Paasonen, P., Stratmann, F., Herrmann, H.,
564   Guenther, A. B., Worsnop, D. R., Kulmala, M., Ehn, M. and Sipilä, M.: Production of extremely low volatile
565   organic compounds from biogenic emissions: Measured yields and atmospheric implications, Proc. Natl. Acad.
566   Sci. U. S. A., 112(23), 7123–7128, doi:10.1073/pnas.1423977112, 2015.
567   Jørgensen, S., Knap, H. C., Otkjær, R. V., Jensen, A. M., Kjeldsen, M. L. H., Wennberg, P. O. and Kjaergaard, H.
568   G.: Rapid Hydrogen Shift Scrambling in Hydroperoxy-Substituted Organic Peroxy Radicals, J. Phys. Chem. A,
569   120(2), 266–275, doi:10.1021/acs.jpca.5b06768, 2016.
570   Krechmer, J., Lopez-Hilfiker, F., Koss, A., Hutterli, M., Stoermer, C., Deming, B., Kimmel, J., Warneke, C.,
571   Holzinger, R., Jayne, J., Worsnop, D., Fuhrer, K., Gonin, M. and De Gouw, J.: Evaluation of a New Reagent-
572   Ion Source and Focusing Ion− Molecule Reactor for Use in Proton-Transfer-Reaction Mass Spectrometry,
573   Anal. Chem., 90, 12011–12018, doi:10.1021/acs.analchem.8b02641, 2018.
574   Krechmer, J. E., Coggon, M. M., Massoli, P., Nguyen, T. B., Crounse, J. D., Hu, W., Day, D. A., Tyndall, G. S.,
575   Henze, D. K., Rivera-Rios, J. C., Nowak, J. B., Kimmel, J. R., Mauldin, R. L., Stark, H., Jayne, J. T., Sipilä,
576   M., Junninen, H., St. Clair, J. M., Zhang, X., Feiner, P. A., Zhang, L., Miller, D. O., Brune, W. H., Keutsch, F.
577   N., Wennberg, P. O., Seinfeld, J. H., Worsnop, D. R., Jimenez, J. L. and Canagaratna, M. R.: Formation of
578   Low Volatility Organic Compounds and Secondary Organic Aerosol from Isoprene Hydroxyhydroperoxide
579   Low-NO Oxidation, Environ. Sci. Technol., 49(17), 10330–10339, doi:10.1021/acs.est.5b02031, 2015.
580   Kroll, J. H. and Seinfeld, J. H.: Chemistry of secondary organic aerosol: Formation and evolution of low-volatility
581   organics in the atmosphere, Atmos. Environ., 42(16), 3593–3624, doi:10.1016/j.atmosenv.2008.01.003, 2008.
582   Kroll, J. H., Donahue, N. M., Jimenez, J. L., Kessler, S. H., Canagaratna, M. R., Wilson, K. R., Altieri, K. E.,
583   Mazzoleni, L. R., Wozniak, A. S., Bluhm, H., Mysak, E. R., Smith, J. D., Kolb, C. E. and Worsnop, D. R.:
584   Carbon oxidation state as a metric for describing the chemistry of atmospheric organic aerosol, Nat. Chem.,
585   3(2), 133–139, doi:10.1038/nchem.948, 2011.
586   Kurylo, M. J. and Orkin, V. L.: Determination of Atmospheric Lifetimes via the Measurement of OH Radical
587   Kinetics, Chem. Rev., 103(12), 5049–5076, doi:10.1021/cr020524c, 2003.
588   Kwok, E. S. C. and Atkinson, R.: Estimation of hydroxyl radical reaction rate constants for gas-phase organic
589   compounds using a structure-reactivity relationship: An update, Atmos. Environ., 29(14), 1685–1695,
590   doi:10.1016/1352-2310(95)00069-B, 1995.
591   Lambe, A., Massoli, P., Zhang, X., Canagaratna, M., Nowak, J., Daube, C., Yan, C., Nie, W., Onasch, T., Jayne, J.,
592   Kolb, C., Davidovits, P., Worsnop, D. and Brune, W.: Controlled nitric oxide production via O(1D) + N2O
593   reactions for use in oxidation flow reactor studies, Atmos. Meas. Tech., 10(6), 2283–2298, doi:10.5194/amt-
594   10-2283-2017, 2017.
595   Lambe, A. T., Krechmer, J. E., Peng, Z., Casar, J. R., Carrasquillo, A. J., Raff, J. D., Jimenez, J. L. and Worsnop, D.
596   R.: HOx and NOx production in oxidation flow reactors via photolysis of isopropyl nitrite, isopropyl nitrite-d

14

597   7 , and 1,3-propyl dinitrite at λ = 254, 350, and 369 nm, Atmos. Meas. Tech., 12(1), 299–311, doi:10.5194/amt-
598   12-299-2019, 2019.
599   Lee, B. H., Lopez-Hilfiker, F. D., Mohr, C., Kurtén, T., Worsnop, D. R. and Thornton, J. A.: An iodide-adduct high-
600   resolution time-of-flight chemical-ionization mass spectrometer: Application to atmospheric inorganic and
601   organic compounds, Environ. Sci. Technol., 48(11), 6309–6317, doi:10.1021/es500362a, 2014.
602   Li, H., Riva, M., Rantala, P., Heikkinen, L., Daellenbach, K., Krechmer, J. E., Flaud, P.-M., Worsnop, D., Kulmala,
603   M., Villenave, E., Perraudin, E., Ehn, M. and Bianchi, F.: Terpenes and their oxidation products in the French
604   Landes forest: insight from Vocus PTR-TOF measurements, Atmos. Chem. Phys. Discuss., (September), 1–29,
605   doi:10.5194/acp-2019-741, 2019.
606   Li, Y. and Wang, L.: The atmospheric oxidation mechanism of 1,2,4-trimethylbenzene initiated by OH radicals,
607   Phys. Chem. Chem. Phys., 16(33), 17908, doi:10.1039/C4CP02027H, 2014.
608   Lopez-Hilfiker, F. D., Mohr, C., Ehn, M., Rubach, F., Kleist, E., Wildt, J., Mentel, T. F., Lutz, A., Hallquist, M.,
609   Worsnop, D. and Thornton, J. A.: A novel method for online analysis of gas and particle composition:
610   Description and evaluation of a filter inlet for gases and AEROsols (FIGAERO), Atmos. Meas. Tech., 7, 983–
611   1001, doi:10.5194/amt-7-983-2014, 2014.
612   Lopez-Hilfiker, F. D., Iyer, S., Mohr, C., Lee, B. H., D'ambro, E. L., Kurtén, T. and Thornton, J. A.: Constraining
613   the sensitivity of iodide adduct chemical ionization mass spectrometry to multifunctional organic molecules
614   using the collision limit and thermodynamic stability of iodide ion adducts, Atmos. Meas. Tech., 9(4), 1505–
615   1512, doi:10.5194/amt-9-1505-2016, 2016.
616   Mentel, T. F., Springer, M., Ehn, M., Kleist, E., Pullinen, I., Kurtén, T., Rissanen, M., Wahner, A. and Wildt, J.:
617   Formation of highly oxidized multifunctional compounds: Autoxidation of peroxy radicals formed in the
618   ozonolysis of alkenes - Deduced from structure-product relationships, Atmos. Chem. Phys., 15(12), 6745–
619   6765, doi:10.5194/acp-15-6745-2015, 2015.
620   Mehra, A., Wang, Y., Krechmer, J. E., Lambe, A., Majluf, F., Morris, M. A., Priestley, M., Bannan, T. J., Bryant, D.
621   J. Pereira, K. L., Hamilton, J. F., Rickard, A., Newland, M., Stark, H., Croteau, P., Jayne, J. T., Worsnop, D.
622   R., Canagaratna, M., R., Wang L., Coe H., Atmos. Chem. Phys., submitted.
623   Molteni, U., Bianchi, F., Klein, F., Haddad, I. El, Frege, C., Rossi, M. J., Dommen, J. and Baltensperger, U.:
624   Formation of highly oxygenated organic molecules from aromatic compounds, Atmos. Chem. Phys, 18, 1909–
625   1921, doi:10.5194/acp-18-1909-2018, 2018.
626   Nah, T., Sanchez, J., Boyd, C. M. and Ng, N. L.: Photochemical Aging of α-pinene and β-pinene Secondary Organic
627   Aerosol formed from Nitrate Radical Oxidation, Environ. Sci. Technol., 50(1), 222–231,
628   doi:10.1021/acs.est.5b04594, 2016.
629   Ng, N. L., Canagaratna, M. R., Zhang, Q., Jimenez, J. L., Tian, J., Ulbrich, I. M., Kroll, J. H., Docherty, K. S.,
630   Chhabra, P. S., Bahreini, R., Murphy, S. M., Seinfeld, J. H., Hildebrandt, L., Donahue, N. M., Decarlo, P. F.,
631   Lanz, V. A., Prévôt, A. S. H., Dinar, E., Rudich, Y. and Worsnop, D. R.: Organic aerosol components observed
632   in Northern Hemispheric datasets from Aerosol Mass Spectrometry, Atmos. Chem. Phys., 10(10), 4625–4641,
633   doi:10.5194/acp-10-4625-2010, 2010.
634   Orlando, J. J. and Tyndall, G. S.: Laboratory studies of organic peroxy radical chemistry: An overview with
635   emphasis on recent issues of atmospheric significance, Chem. Soc. Rev., 41(19), 6294–6317,
636   doi:10.1039/c2cs35166h, 2012.
637   Otkjær, R. V., Jakobsen, H. H., Tram, C. M. and Kjaergaard, H. G.: Calculated Hydrogen Shift Rate Constants in
638   Substituted Alkyl Peroxy Radicals, J. Phys. Chem. A, 122(43), 8665–8673, doi:10.1021/acs.jpca.8b06223,
639   2018.
640   Peng, Z., Day, D. A., Stark, H., Li, R., Lee-Taylor, J., Palm, B. B., Brune, W. H. and Jimenez, J. L.: HO x radical
641   chemistry in oxidation flow reactors with low-pressure mercury lamps systematically examined by modeling,
642   Atmos. Meas. Tech, 8, 4863–4890, doi:10.5194/amt-8-4863-2015, 2015.
643   Richters, S., Herrmann, H. and Berndt, T.: Different pathways of the formation of highly oxidized multifunctional
644   organic compounds (HOMs) from the gas-phase ozonolysis of β-caryophyllene, Atmos. Chem. Phys., 16(15),
645   9831–9845, doi:10.5194/acp-16-9831-2016, 2016.
646   Rissanen, M. P.: NO2 Suppression of Autoxidation-Inhibition of Gas-Phase Highly Oxidized Dimer Product
647   Formation, ACS Earth Sp. Chem., 2(11), 1211–1219, doi:10.1021/acsearthspacechem.8b00123, 2018.
648   Rissanen, M. P., Kurtén, T., Sipilä, M., Thornton, J. A., Kangasluoma, J., Sarnela, N., Junninen, H., Jørgensen, S.,
649   Schallhart, S., Kajos, M. K., Taipale, R., Springer, M., Mentel, T. F., Ruuskanen, T., Petäjä, T., Worsnop, D.
650   R., Kjaergaard, H. G. and Ehn, M.: The formation of highly oxidized multifunctional products in the ozonolysis
651   of cyclohexene, J. Am. Chem. Soc., 136(44), 15596–15606, doi:10.1021/ja507146s, 2014.
652   Rissanen, M. P., Kurtén, T., Sipilä, M., Thornton, J. A., Kausiala, O., Garmash, O., Kjaergaard, H. G., Petäjä, T.,

Worsnop, D. R., Ehn, M. and Kulmala, M.: Effects of chemical complexity on the autoxidation mechanisms of endocyclic alkene ozonolysis products: From methylcyclohexenes toward understanding α-pinene, J. Phys. Chem. A, 119(19), 4633–4650, doi:10.1021/jp510966g, 2015.

Riva, M., Rantala, P., Krechmer, J. E., Peräkylä, O., Zhang, Y., Heikkinen, L., Garmash, O., Yan, C., Kulmala, M., Worsnop, D. and Ehn, M.: Evaluating the performance of five different chemical ionization techniques for detecting gaseous oxygenated organic species, Atmos. Meas. Tech, 12, 2403–2421, doi:10.5194/amt-12-2403-2019, 2019.

Saunders, S. M., Jenkin, M. E., Derwent, R. G. and Pilling, M. J.: Protocol for the development of the Master Chemical Mechanism, MCM v3 (Part A): Tropospheric degradation of non-aromatic volatile organic compounds, Atmos. Chem. Phys., 3(1), 161–180, doi:10.5194/acp-3-161-2003, 2003.

Stolzenburg, D., Fischer, L., Vogel, A. L., Heinritzi, M., Schervish, M., Simon, M., Wagner, A. C., Dada, L., Ahonen, L. R., Amorim, A., Baccarini, A., Bauer, P. S., Baumgartner, B., Bergen, A., Bianchi, F., Breitenlechner, M., Brilke, S., Mazon, S. B., Chen, D., Dias, A., Draper, D. C., Duplissy, J., Haddad, I. El, Finkenzeller, H., Frege, C., Fuchs, C., Garmash, O., Gordon, H., He, X., Helm, J., Hofbauer, V., Hoyle, C. R., Kim, C., Kirkby, J., Kontkanen, J., Kürten, A., Lampilahti, J., Lawler, M., Lehtipalo, K., Leiminger, M., Mai, H., Mathot, S., Mentler, B., Molteni, U., Nie, W., Nieminen, T., Nowak, J. B., Ojdanic, A., Onnela, A., Passananti, M., Petäjä, T., Quéléver, L. L. J., Rissanen, M. P., Sarnela, N., Schallhart, S., Tauber, C., Tomé, A., Wagner, R., Wang, M., Weitz, L., Wimmer, D., Xiao, M., Yan, C., Ye, P., Zha, Q., Baltensperger, U., Curtius, J., Dommen, J., Flagan, R. C., Kulmala, M., Smith, J. N., Worsnop, D. R., Hansel, A., Donahue, N. M. and Winkler, P. M.: Rapid growth of organic aerosol nanoparticles over a wide tropospheric temperature range, Proc. Natl. Acad. Sci. U. S. A., 115(37), 9122–9127, doi:10.1073/pnas.1807604115, 2018.

Teng, A. P., Crounse, J. D. and Wennberg, P. O.: Isoprene Peroxy Radical Dynamics, J. Am. Chem. Soc., 139(15), 5367–5377, doi:10.1021/jacs.6b12838, 2017.

Tröstl, J., Chuang, W. K., Gordon, H., Heinritzi, M., Yan, C., Molteni, U., Ahlm, L., Frege, C., Bianchi, F., Wagner, R., Simon, M., Lehtipalo, K., Williamson, C., Craven, J. S., Duplissy, J., Adamov, A., Almeida, J., Bernhammer, A. K., Breitenlechner, M., Brilke, S., Dias, A., Ehrhart, S., Flagan, R. C., Franchin, A., Fuchs, C., Guida, R., Gysel, M., Hansel, A., Hoyle, C. R., Jokinen, T., Junninen, H., Kangasluoma, J., Keskinen, H., Kim, J., Krapf, M., Kürten, A., Laaksonen, A., Lawler, M., Leiminger, M., Mathot, S., Möhler, O., Nieminen, T., Onnela, A., Petäjä, T., Piel, F. M., Miettinen, P., Rissanen, M. P., Rondo, L., Sarnela, N., Schobesberger, S., Sengupta, K., Sipilä, M., Smith, J. N., Steiner, G., Tomè, A., Virtanen, A., Wagner, A. C., Weingartner, E., Wimmer, D., Winkler, P. M., Ye, P., Carslaw, K. S., Curtius, J., Dommen, J., Kirkby, J., Kulmala, M., Riipinen, I., Worsnop, D. R., Donahue, N. M. and Baltensperger, U.: The role of low-volatility organic compounds in initial particle growth in the atmosphere, Nature, 533(7604), 527–531, doi:10.1038/nature18271, 2016.

Tsiligiannis, E., Hammes, J., Salvador, C. M., Mentel, T. F. and Hallquist, M.: Effect of NOx on 1,3,5-trimethylbenzene (TMB) oxidation product distribution and particle formation, Atmos. Chem. Phys., 19(23), 15073–15086, doi:10.5194/acp-19-15073-2019, 2019.

Wang, S., Wu, R., Berndt, T., Ehn, M. and Wang, L.: Formation of Highly Oxidized Radicals and Multifunctional Products from the Atmospheric Oxidation of Alkylbenzenes, Environ. Sci. Technol., 51(15), 8442–8449, doi:10.1021/acs.est.7b02374, 2017.

Wang, Y., Riva, M., Xie, H. and Heikkinen, L.: Formation of highly oxygenated organic molecules from chlorine atom initiated oxidation of alpha-pinene, Atmos. Chem. Phys. Discuss., (October), 1–31, doi:10.5194/acp-2019-807, 2019.

Yuan, B., Koss, A. R., Warneke, C., Coggon, M., Sekimoto, K. and De Gouw, J. A.: Proton-Transfer-Reaction Mass Spectrometry: Applications in Atmospheric Sciences, Chem. Rev., 117(21), 13187–13229, doi:10.1021/acs.chemrev.7b00325, 2017.

Zaytsev, A., Koss, A. R., Breitenlechner, M., Krechmer, J. E., Nihill, K. J., Lim, C. Y., Rowe, J. C., Cox, J. L., Moss, J., Roscioli, J. R., Canagaratna, M. R., Worsnop, D. R., Kroll, J. H. and Keutsch, F. N.: Mechanistic study of the formation of ring-retaining and ring-opening products from the oxidation of aromatic compounds under urban atmospheric conditions, Atmos. Chem. Phys., 19(23), 15117–15129, doi:10.5194/acp-19-15117-2019, 2019.

Zhang, Q., Jimenez, J. L., Canagaratna, M. R., Allan, J. D., Coe, H., Ulbrich, I., Alfarra, M. R., Takami, A., Middlebrook, A. M., Sun, Y. L., Dzepina, K., Dunlea, E., Docherty, K., DeCarlo, P. F., Salcedo, D., Onasch, T., Jayne, J. T., Miyoshi, T., Shimono, A., Hatakeyama, S., Takegawa, N., Kondo, Y., Schneider, J., Drewnick, F., Borrmann, S., Weimer, S., Demerjian, K., Williams, P., Bower, K., Bahreini, R., Cottrell, L., Griffin, R. J., Rautiainen, J., Sun, J. Y., Zhang, Y. M. and Worsnop, D. R.: Ubiquity and dominance of oxygenated species in

Atmospheric
Chemistry
and Physics
Discussions

709   organic aerosols in anthropogenically-influenced Northern Hemisphere midlatitudes, Geophys. Res. Lett.,
710   34(13), 1–6, doi:10.1029/2007GL029979, 2007.
711   Zhao, Y., Thornton, J. A. and Pye, H. O. T.: Quantitative constraints on autoxidation and dimer formation from
712   direct probing of monoterpene-derived peroxy radical chemistry, Proc. Natl. Acad. Sci., 115(48), 12142–
713   12147, doi:10.1073/pnas.1812147115, 2018.
714   Ziemann, P. J. and Atkinson, R.: Kinetics, products, and mechanisms of secondary organic aerosol formation,
715   Chem. Soc. Rev., 41(19), 6582–6605, doi:10.1039/c2cs35122f, 2012.

Table 1 Summary of experimental conditions.

#	Precursor	Experimental condition	Precursor concentration (ppb)	Consumption of precursor (%)	RH (%)	Total flow rate (slpm)	O_3 concentration (ppb)
1	1,2,4-TMB	OH	158	59.3	12.5	10	712
2	1,3,5-TMB	OH	118	62.8	13.6	10	845
3	1,2,3-TMB	OH	214	58.4	8.1	10	1426
4	1,2,4-(1-methyl-D3)-TMB	OH	155	62.0	11.6	10	1003
5	1,2,4-(2-methyl-D3)-TMB	OH	169	61.8	12.5	10	776
6	1,2,4-(4-methyl-D3)-TMB	OH	166	62.8	11.5	10	886
7	1,2,4-TMB	Low NO_x (0.8ppb NO_x)	170	61.5	12.7	10.4	944
8	1,2,4-TMB	Higher NO_x (6.5ppb NO_x)	145	69.7	9.3	10.4	3911

Table 2. Oxidation products of 1,2,4-TMB in categories of carbonyl, hydroxyl, and hydroperoxyl according to their molecular mass, as well as the potential peroxy radicals. Numbers in the parenthesis denote the relative intensity detected by Nitrate CI-APi-TOF in the OH-initiated oxidation of 1,2,4-TMB when that of the largest HOM signal ($C_9H_{16}O_8$) is arbitrarily set to be 100%. The relative intensity has been corrected with the relative transmission efficiency of Nitrate CI-APi-TOF.

The potential peroxy radical m	Carbonyl m-17	Hydroxyl m-15	Hydroperoxyl m+1
$C_9H_{13}O_7\cdot$	$C_9H_{12}O_6$ [a,b,c,d] (9.2 %)	$C_9H_{14}O_6$ [a,b,c,d] (20.3 %)	$C_9H_{14}O_7$ [b,c,d] (50.4 %)
$C_9H_{13}O_8\cdot$	$C_9H_{12}O_7$ [b,c,d] (54.4 %)	$C_9H_{14}O_7$ [b,c,d] (50.4 %)	$C_9H_{14}O_8$ [c,d] (51.6 %)
$C_9H_{13}O_9\cdot$	$C_9H_{12}O_8$ [d] (17.3 %)	$C_9H_{14}O_8$ [c,d] (51.6 %)	$C_9H_{14}O_9$ [d] (29.1 %)
$C_9H_{13}O_{10}\cdot$	$C_9H_{12}O_9$ [d] (14.9 %)	$C_9H_{14}O_9$ [d] (29.1 %)	$C_9H_{14}O_{10}$ [d] (19.8 %)
$C_9H_{15}O_7\cdot$	$C_9H_{14}O_6$ [a,b,c,d] (20.3 %)	$C_9H_{16}O_6$ [b,c,d] (2.3 %)	$C_9H_{16}O_7$ [b,c,d] (23.5 %)
$C_9H_{15}O_8\cdot$	$C_9H_{14}O_7$ [b,c,d] (50.4 %)	$C_9H_{16}O_7$ [b,c,d] (23.5 %)	$C_9H_{16}O_8$ [c,d] (100 %)
$C_9H_{15}O_9\cdot$	$C_9H_{14}O_8$ [c,d] (51.6 %)	$C_9H_{16}O_8$ [c,d] (100 %)	$C_9H_{16}O_9$ [d] (40.5 %)
$C_9H_{15}O_{10}\cdot$	$C_9H_{14}O_9$ [d] (29.1 %)	$C_9H_{16}O_9$ [d] (40.5 %)	$C_9H_{16}O_{10}$ [d] (7.1 %)

[a] These compounds are listed in the MCM mechanism of 1,2,4-TMB where they are formed by multiple OH oxidation steps.

[b] These compounds were detected by Vocus PTR.

[c] These compounds were detected by Iodide CI-TOF in both gas and particle phase.

[d] These compounds were detected by Nitrate CI-APi-TOF.

Table 3. Partially deuterated C9 products observed by Vocus PTR and/or Nitrate CI-APi-TOF. "V" and "N" denote observation by Vocus PTR and Nitrate CI-APi-TOF, respectively, whereas "-" means that the product was not observed by any instrument.

	1,2,4-(1-methyl-D3)-TMB	1,2,4-(2-methyl-D3)-TMB	1,2,4-(4-methyl-D3)-TMB
$C_9H_{10}D_2O_6$	V, N	-	-
$C_9H_{10}D_2O_7$	V	-	-
$C_9H_{12}D_2O_8$	-	-	N

Scheme Captions

Scheme 1. A proposed autoxidation reaction scheme involving a bicyclic peroxy radical of $C_9H_{13}O_5 \bullet$.

Scheme 2. A proposed autoxidation reaction scheme involving a bicyclic peroxy radical of $C_9H_{13}O_5 \bullet$. Note that the reaction has been terminated with the formation of $C_9H_{14}O_4$ and re-initiated by a second OH attack.
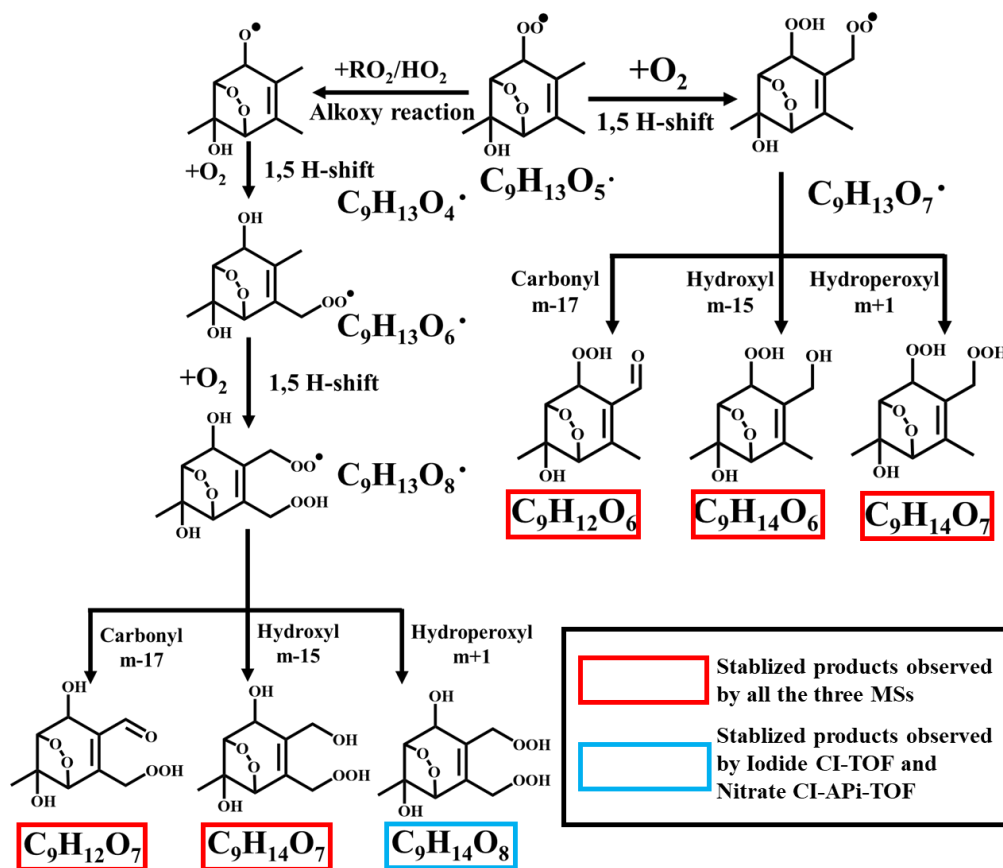
Scheme 1
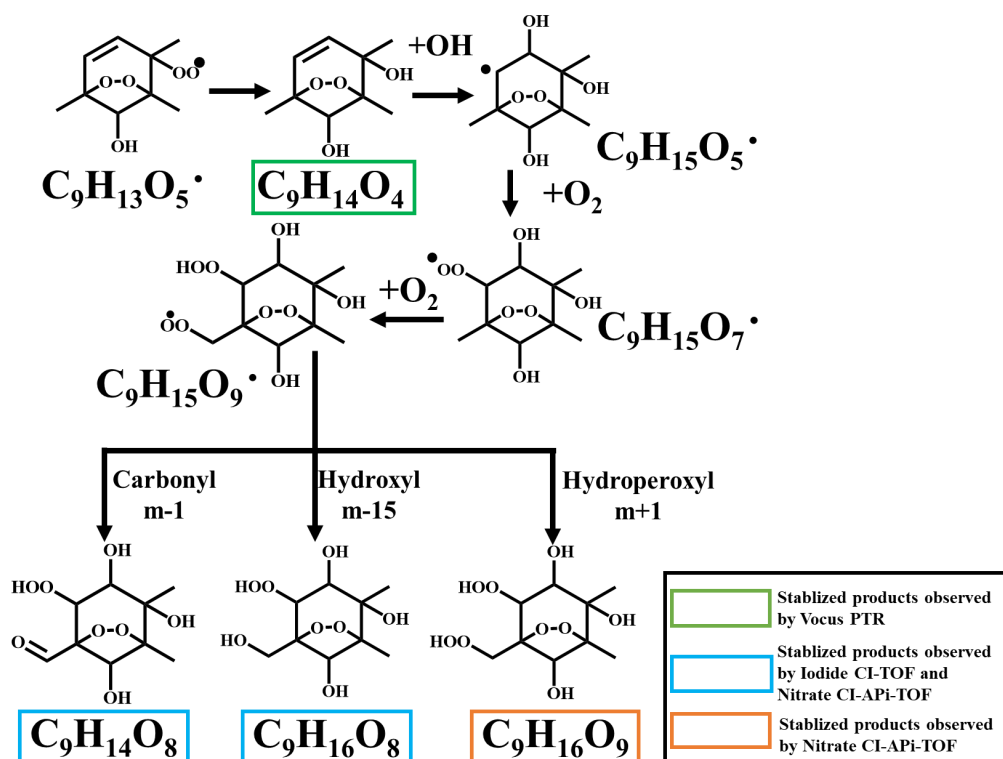
Scheme 2

Figure Captions

Figure 1. Schematics of experimental setup.

Figure 2. Comparison of C7-C9 products observed in the OH-initiated oxidation of 1,2,4-TMB (Exp. #1 in Table 1) with those listed in the MCM mechanism (Bloss et al., 2005). Filled red, orange, and green circles denote observation by Nitrate CI-APi-TOF, Iodide CI-TOF, and Vocus PTR, respectively, whereas open blue circles represent MCM species. The radius of filled circles are proportional to the signals of the compounds in each instrument. The signal of the most abundant product for each instrument is arbitrarily set to be 100%, but note that the arbitrary signals are not comparable among instruments. Symbols have been offset horizontally to avoid overlap.

Figure 3. Distribution of C9 products formed from OH-initiated reactions of TMBs (Exp. #1- 3 in Table 1) by (a) Vocus PTR, (b) Iodide CI-TOF for the gas phase, (c) Iodide CI-TOF for particle phase, and (d) Nitrate CI-APi-TOF. The yield of the most abundant product for each instrument is arbitrarily set to be 100%, but note that the arbitrary yields are not comparable among instruments. Also note that signal of Vocus PTR was processed in a logarithmic way before calculating the arbitrary yield.

Figure 4. (a) Distribution of $C_{18}H_{24}O_{8-13}$ and $C_{18}H_{26}O_{8-15}$ products formed from TMB oxidation experiments (Exp. #1-3 in Table 1), as measured by Nitrate CI-APi-TOF; (b) Distribution of $C_{18}H_{28}O_{9-15}$ and $C_{18}H_{30}O_{12-15}$ formed from TMB oxidation experiments (Exp. #1-3 in Table 1), as measure by Nitrate CI-APi-TOF; and (c) The total signal of C18 products formed from TMB oxidation experiments (Exp. #1-3 in Table 1), as measure by Nitrate CI-APi-TOF.

Figure 5. Relative contribution of C9 and C18 products formed from TMB oxidation experiments, as measured by Nitrate CI-APi-TOF. The relative intensity has been corrected with the relative transmission efficiency.

Figure 6. Comparison of C9 products detected by Nitrate CI-APi-TOF with zero, one or two nitrogen atoms formed from 1,2,4-TMB oxidation with different NO_x settings.

Figure 7. (a) Comparison of C18 HOMs formed from 1,2,4-TMB oxidation with different NO_x settings; and (b) Distribution of C18 organonitrates fomed from 1,2,4-TMB oxidation.
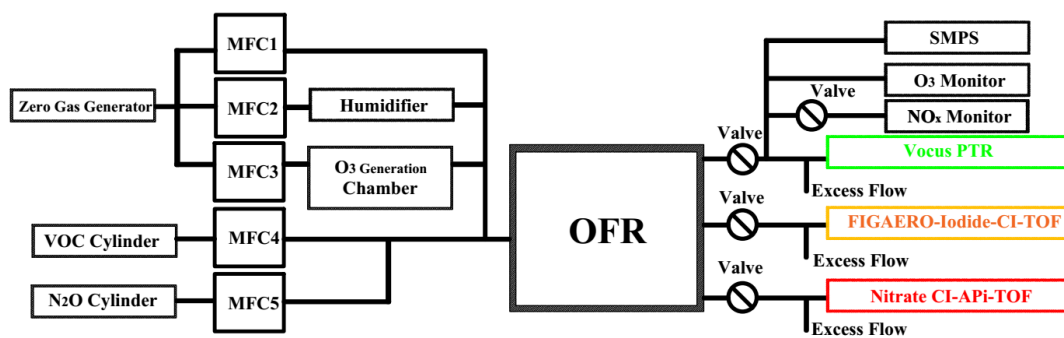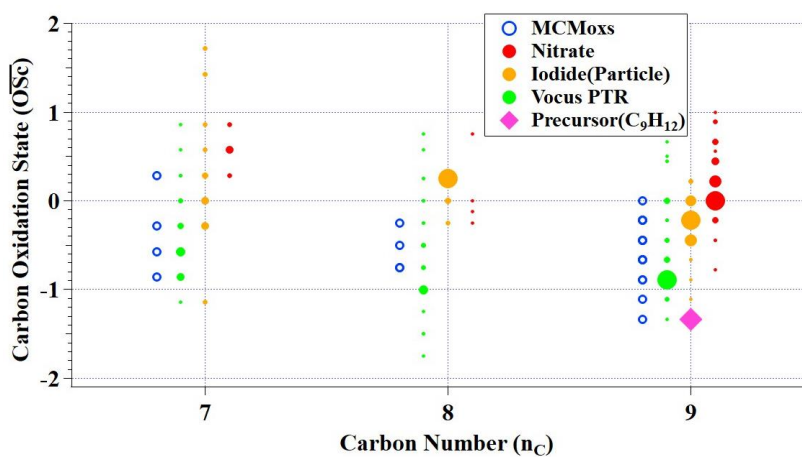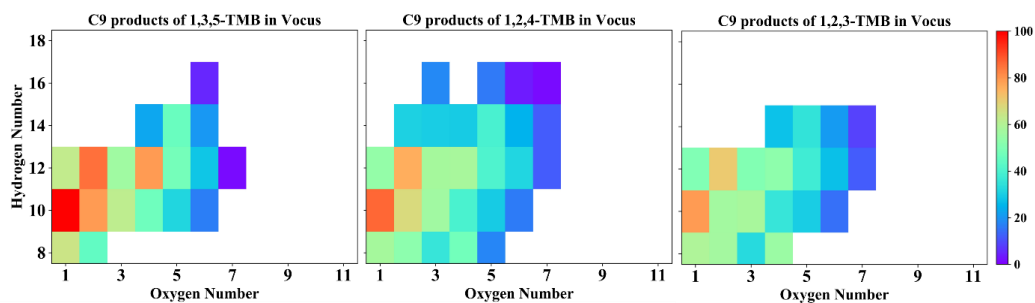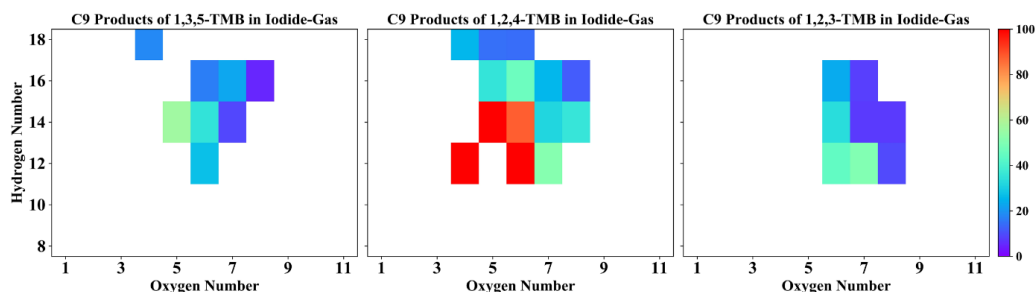
Figure 1

Figure 2

Figure 3a

Figure 3b
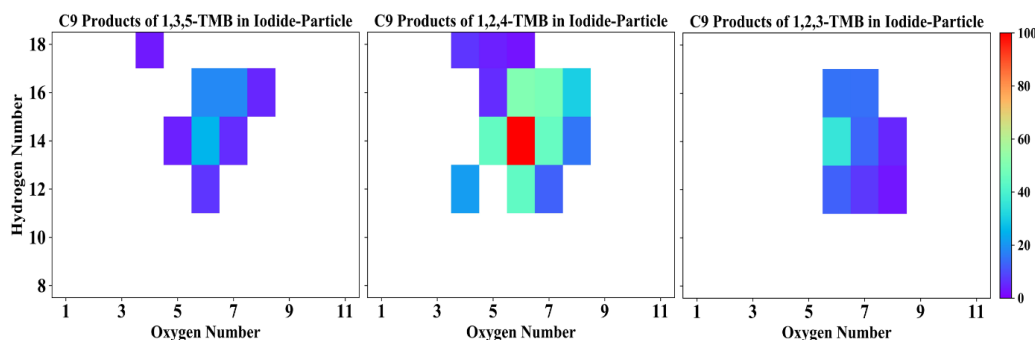
Figure 3c
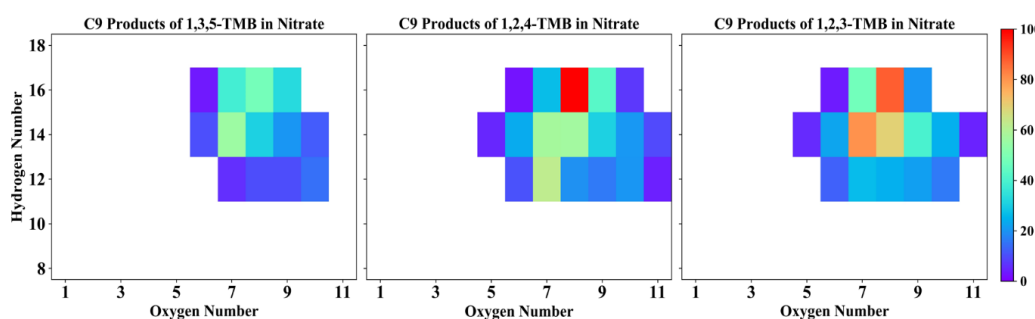
Figure 3d
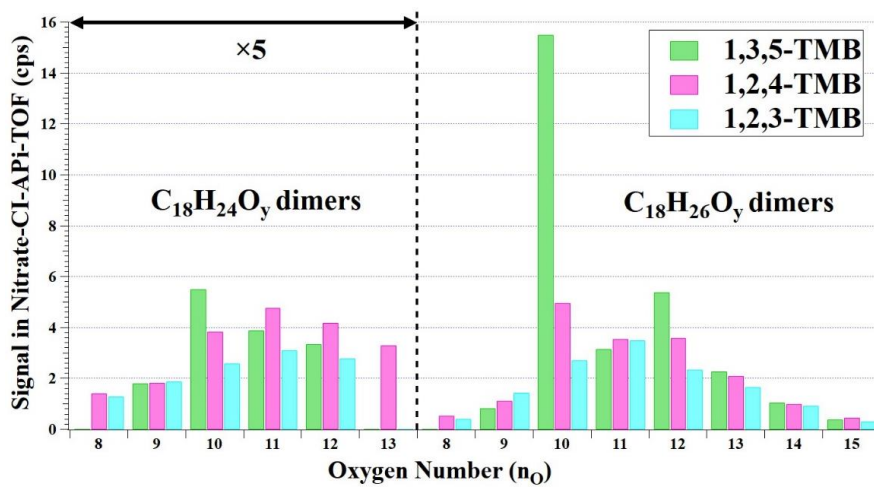
Figure 4a
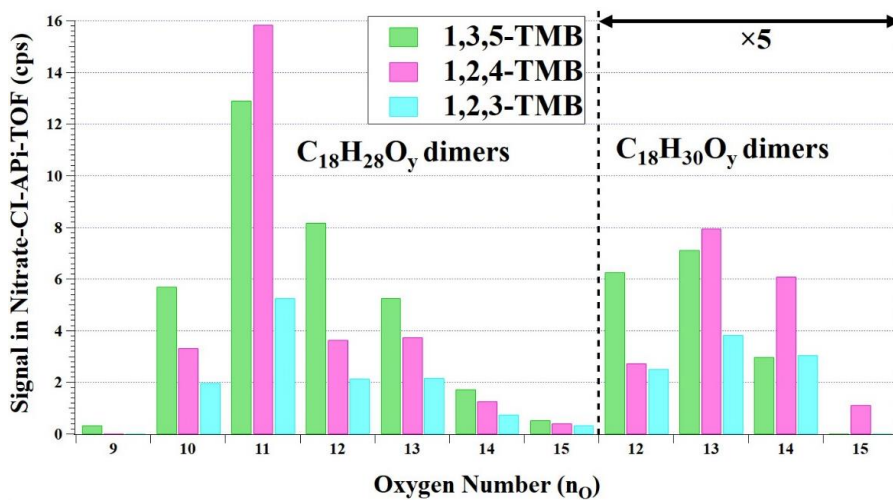
Figure 4b

Figure 4c
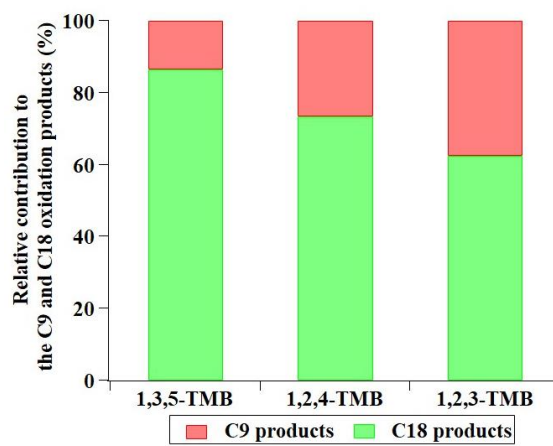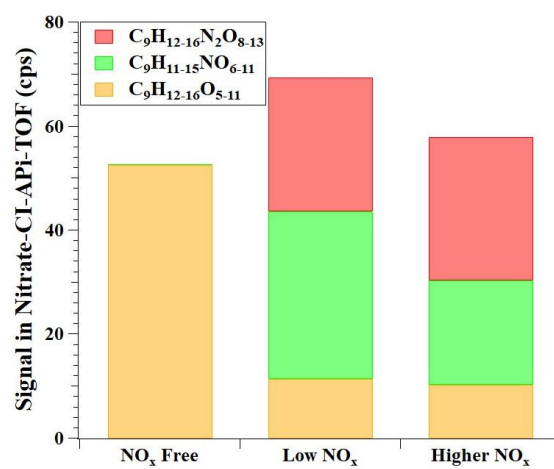
Figure 5

Atmospheric
Chemistry
and Physics
Discussions

Open Access

EGU
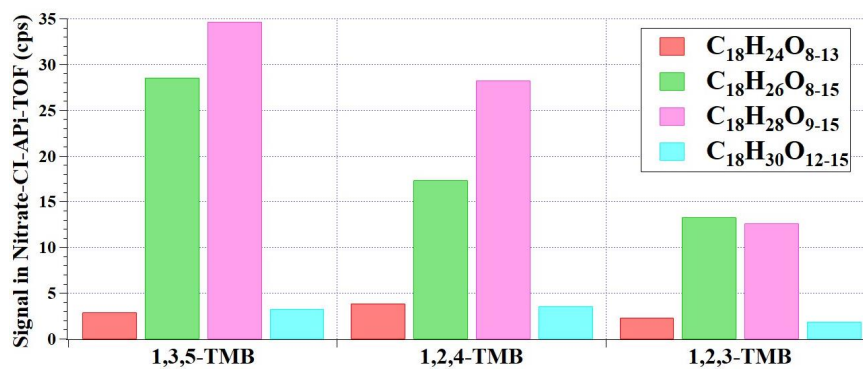
Figure 6

Figure 7a

Figure 7b